White Paper X

A Theoretical Interpretation of Non-Local, Spatial, Room Temperature, Macroscopic Size Information Entanglement

by:

William A. Tiller Ph.D. and W. E. Dibble, Jr.

This White Paper was originally Part III in the presently 5-part series of papers entitled "Towards General Experimentation and Discovery in "Conditioned Laboratory Spaces" of which the other four were all published in the Journal of Alternative and Complementary Medicine (JACM).

A Theoretical Interpretation of Non-Local, Spatial, Room Temperature, Macroscopic Size Information Entanglement

by

W. A. Tiller and W.E. Dibble, Jr.

Abstract

Our conventional reference frame (RF) for viewing nature, spacetime, is unable to account for the experimental data provided in Parts I and II so a new RF is utilized. This biconformal base-space (BFBS) RF, consists of two, four-dimensional, reciprocal subspaces wherein one is spacetime, imbedded in the three higher dimensions of emotion, mind and spirit. This model has the quantitative capacity that allows us to understand the new data. This particular BCBS generates (1) simultaneous particle and information wave behavior, (2) connectedness between any two points of spacetime, (3) non-local forces, (4) dual aspects of any measured material property, one from each subspace, with the magnitude ratio of the two aspects depending upon a higher dimensional coupling medium that can be modulated by human intention and (5) non-local information entanglement between any two parts of the overall consciousness-connected system.

Utilizing the measured pH(t)-data, this BCBS reference frame is utilized to calculate the spectral amplitude profile of the reciprocal-space aspect as well as the magnitude of the direct-space aspect. This BCBS reference frame is also utilized in a quantitative way to show how information entanglement naturally comes about when the experimental system consists of multiple parts. The various quantitative factors involved in calculating magnitudes of information entanglement between non-local sites, having different degrees of departure from the U(1) EM gauge symmetry state, are demonstrated.

Introduction

The general background for this paper has evolved over the past 30-40 years with various encapsulations by us[1-9] and others[10,11]. In particular, reference 8 provides the briefest underpinning for this paper. In part I[12] of this series it was shown that, when fresh purified water was placed in a pH-measurement vessel at a variety of partially "conditioned" sites, the change in pH with time was either exponential or linear in nature. Although some hints of non-local information

entanglement was suggested on page 190 of reference 6, here we find robust initial evidence for its occurrence between the various IIED sites and their "control" sites ~2-20 miles away. In Part II[13], further strong evidence was found for non-local information entanglement between sites that were 1000-2000 miles separated from any IIED site in the overall experimental system. Further, it was apparent from the very outset that this information transfer was occurring via a non-electromagnetic pathway, at least in a conventional electromagnetism sense. This is so for the following reason. We take two physically identical devices but one is an IIED and the other has not been intention imprinted. In the electrically "off" state, they are separated by ~100 meters and we find that, by some new type of communication channel, the imprint intention from the IIED is broadcast to the unimprinted "control" device and one essentially loses the "control". Thus, as we seek an explanation for non-local information entanglement as well as for the exponential and linear time dependence of pH-change at all sites, we cannot depend on conventional electromagnetism as the primary mechanism.

In the next section, we utilize the general biconformal base-space theory[1,6,8,9] to recognize that the magnitude of every physical measurement consists of two conjugate portions, a direct space part and a deltron-empowered reciprocal space part. We then calculate the spectral profile of the reciprocal space portion needed to agree with the experimental pH-time dependence reported in Part I. In the following section, we utilize the same basic theoretical model to show how non-local information entanglement is a natural consequence of such a model and demonstrate many quantitative aspects of the theory. In passing, one is readily able to see one source of the placebo effect in medicine.

A. Converting from Time-domain Measurements to R-space spectral Amplitude Profiles

Since our particular biconformal base-space is constructed from two reciprocal 4-spaces, D-space and R-space, respectively, where D-space is distance-time (x,y,z,t) Fourier-pair relationships are mathematically required to exist between the two conjugate qualities of substance in D-space and R-space. Thus, for any physical pH measurement, $Q_{M_{pH}}$, given, for example, by

$$Q_{M_{pH}} = pH_0 + \Delta pH(1 - e^{-\beta t}) \tag{1a}$$

or

$$Q_{M_{pH}} = pH_0 + \gamma t \tag{1b}$$

as determined experimentally in Part I[12], we must choose the following format

$$Q_{M_{pH}} = Q_{D_{pH}} + Q_{R_{pH}}, \tag{2a}$$

and the usual decision is how to split up Equation 1a or 1b into the two parts that comprise the right side of Equation 2a. In this particular case, the decision is an easy one since pH_0 is the theoretically calculated value for pure water in equilibrium with air at temperature T and the local ambient carbon dioxide concentration ($\sim 10^{-3.5}$ atmospheres) under the unstated assumption that the local ambient space is at the U(1) electromagnetic (EM) gauge symmetry level; i.e.,

$$Q_{D_{pH}} \approx pH_0. \qquad (2b)$$

The approximation sign rather than the equal sign must be used here because, even for our normal reality, the U(1) EM gauge symmetry state, $Q_{R_{pH}}$ is not equal to zero but it is very much smaller than $Q_{D_{pH}}$. Thus, comparing equation 2a with Equations 2b and 1, we know that

$$Q_{R_{pH}} \approx \Delta pH(1-e^{-\beta t}) \text{ or} \qquad (2c)$$

$$Q_{R_{pH}} \approx \gamma t. \qquad (2d)$$

Now we must mathematically work with the Fourier-pair relationships, using Equations 2c or 2d, in order to derive the deltron-empowered, spectral amplitude of

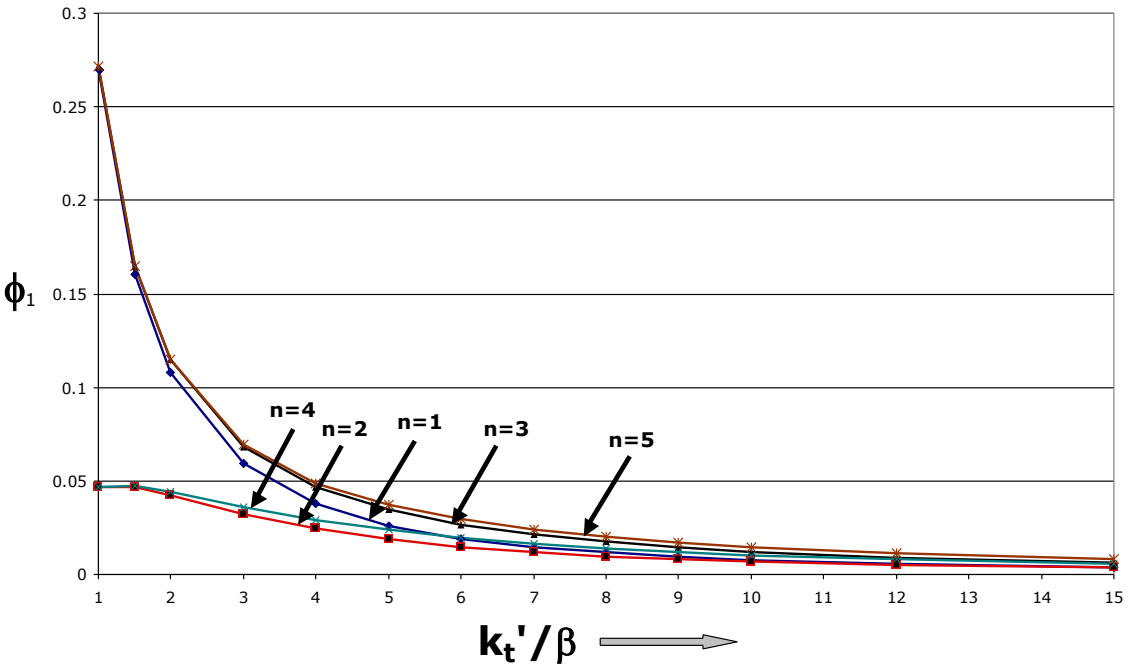

$Q_{R_{pH}}$

Figure 1a $\phi_1 = \hat{I}^2_{R_{pH}}\,\beta/v^*\Delta pH$ vs. k'_t/β plots of the first five allowed solutions, n, from Equation I-8a and the definition of x for a given y (starting at y=1).

(Equation 2c) in R-space, $\hat{I}_{R_{pH}}$. This procedure is carried out in Appendix I and Appendix II (Equation 2d) for those who are mathematically inclined. Here, we present the results for Equation 2c, which is richer than Equation 2d, and we present the results for Equation 2d as well. One readily sees the relationship between these equations because the value of Equation 2c at small times is the same as Equation 2d with $\gamma \approx \beta\Delta\square\square$. Figure 1a shows a plot of the parameter $\phi = \hat{I}^2_{R_{pH}}\,\beta/v^*\Delta pH$ as a function of the dimensionless reciprocal space coordinate, k'_t/β, for the first five allowed solutions n=1, 2, 3, 4, 5 to the Equations of Appendix I.

Figure 1b shows the analytical result from Equation II-5 with $\phi_2 = \hat{I}^2_{R_{pH}}/v^*\gamma$, $t=2\pi/k'_t$ and n=0, +1, +2, …+100. The definition of ϕ in Figures 1a and 1b is slightly different explaining why the scales are so different between the two Figures. The ratio of the two ϕ–values, $\phi_1/\phi_2 = \gamma\beta/\Delta pH$, requires ϕ_1 in Figure 1a to be divided by $\gamma\beta$, assuming $\Delta pH \sim 1$. Since the values of γ range from ~0.001 to 0.01 and the values of β range from ~0.005 to 0.015, the ϕ_1 scale of Figure 1a needs to be increased by a factor of ~10000 to make it comparable to the ϕ_2-scale of Figure 1b. Likewise, the k'_t–scale of

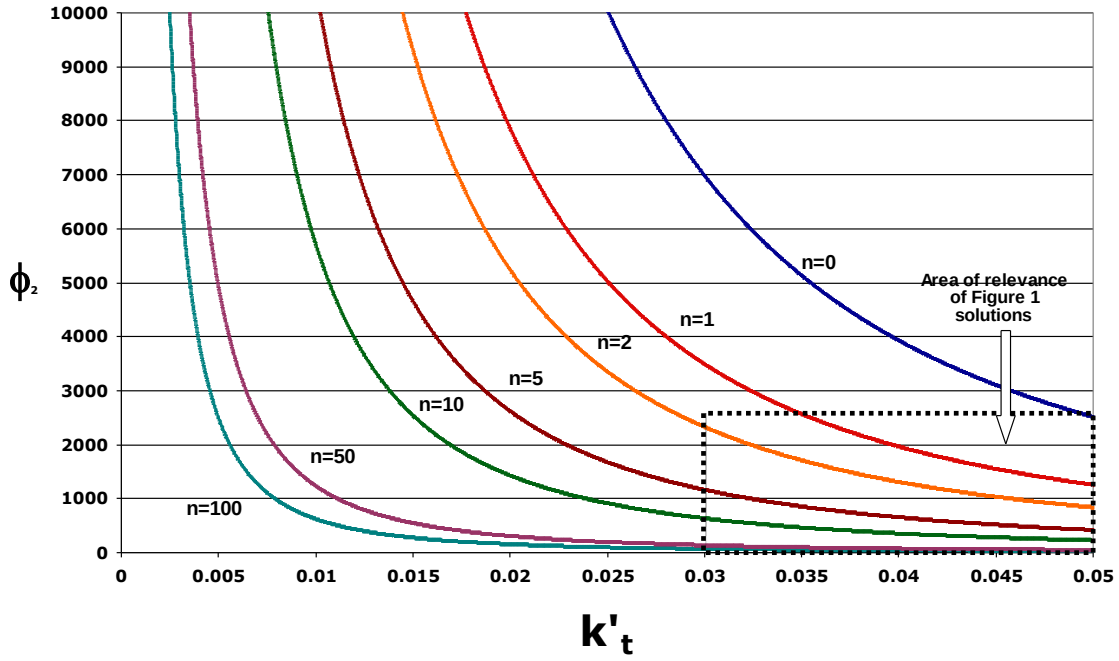

Figure 1b $\phi_2 = \hat{I}^2_{R_{pH}}/v^*\gamma$ as a function of k'_t for $0 \le n \le 100$.

Figure 1b needs to be multiplied by ~100 to make it comparable to the k'_t/β scale of Figure 1a. With these ranges of key parameters in mind, the area of relevance of the Figure 1a solutions, shown on the far right in Figure 1b, becomes clearer. Figures 1a and 1b are very similar in shape although Figure 1b exhibits a little more complexity, as might be expected from an exponential vs. a linear time dependence for the D-space portion. Perhaps the bottom-line conclusion to be drawn from these two plots is that $\hat{I}_{R_{pH}}$ is almost inversely proportional to $n^{1/2}\ k'_t$. Interestingly enough, increasing n causes ϕ_2, in Figure 1b, to decrease while, in Figure 1b, it increases for odd values of n but decreases for even values of n. If we confine ourselves to the n=1 solution, no discrepancy occurs between the ϕ_1 and ϕ_2 plots.

Such plots provide us with the deltron-empowered spectral R-space amplitude, $\hat{I}_{R_{pH}}$, as a function of R-space frequency, $k'_t = 2\pi/t$, in terms of the experimental parameters for each site, β and ΔpH, plus an undetermined velocity, v*, which represents the velocity of our reference frame (the moving earth) through the cosmos. We shall arbitrarily choose n=1 as our preferred solution until new information suggests otherwise. Although we have the R-space spectral amplitude via the procedures of Appendix I, we are unable to gain deltron-empowered phase angle information, $\hat{\theta}(k'_t)$, as function of the R-space frequency coordinate, k'_t. Thus, we are unable to completely describe the vectorial character of the R-space spectral profile. Further, we are at present unable to utilize Equation I-2b of Appendix I to

obtain relevant information concerning the deltron activation function required for an internally self-consistent match with the experimental data, $Q_{M_{pH}}(t)$.

B. R-space Information Entanglement between Remote Sites

(a) Relevant Background

In previous work[6] (see Chapter 7, Figures 7.6 to 7.9), we evaluated the R-space modulus for a fairly wide variety of shaped objects utilizing a continuum approximation for the substance distribution throughout the volume. We also evaluated a granular approximation for a thin triangular-shaped object as being composed of a group of small circular disks of continuum material in a close-packed arrangement (see Figure 2).

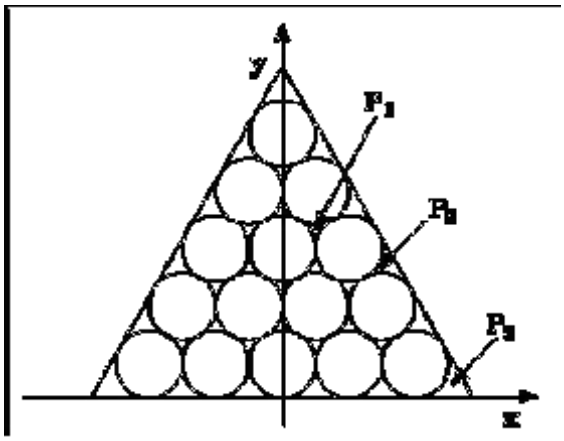

Figure 2 Illustration of the uniformly dense circles granularity approximation compared to the continuum approximation for a thin triangular sheet (the P_j are the three kinds of pores).

In order to evaluate the system Fourier transform (FT) for this group of disks, all at the same electromagnetic (EM) gauge symmetry state, one finds the spatial coordinates for the center of each disk, then the FT for each disk about its center, then the change in the FT to FT' due to a simple translation of the disk center from (0,0,0) to the position $(\bar{x},\bar{y},\bar{z})$ and then add up all the FT's for all the disks in the triangle (relative to the centroid of the triangle for example). For this disk translation, we have

$$FT'(k_x,k_y,k_z) = e^{i(\bar{x}k_x+\bar{y}k_y+\bar{z}k_z)}\, FT(k_x,k_y,k_z). \qquad (3)$$

The value of choosing the centroid as the origin of the system is that then the system Fourier transform, FT_S, is mathematically real. Any other choice of origin for the system leads to mathematically imaginary contributions to FT_S. For (2N+1) close-packed disks in the triangle one finds that, even at N=2, the six-fold arm pattern normal to each side of the triangle is present but, instead of stretching to $\bar{k} \to \infty$ as in the continuum approximation, the length of these arms is small. We have found[6] that the arm length in R-space increases as N increases; i.e., as the radius of the disk becomes smaller and smaller relative to the edge length of the triangle. However, because of the excluded pore area in Figure 2, shrinking the disk radius to zero, as in the continuum approximation, gives a slightly different quantitative result for this

granular approximation than for the continuum approximation.

A second important piece of background that is needed before we tackle the main analytical process path of this section also comes from earlier work[6] (see Chapter 6, Figures 6.15). Figure 3 indicates the geometrical and spatial arrangement of four experimental sites, A to D, involved in this particular Minnesota study. Temperature and pH were recorded at each site using purified water with a small addition of $ZnCO_3$ colloidal-sized particulates as the intention transmitting and receiving medium. All the water vessels were <u>inside</u> individual, electrically-grounded Faraday cages; however, the actual pH-meters were outside the cages at all four sites. Site B had been "conditioned" before any others but a pH-lowering IIED was placed only at A and operated in such a way as to create a train of pH-oscillations. After a short time, the following was observed:

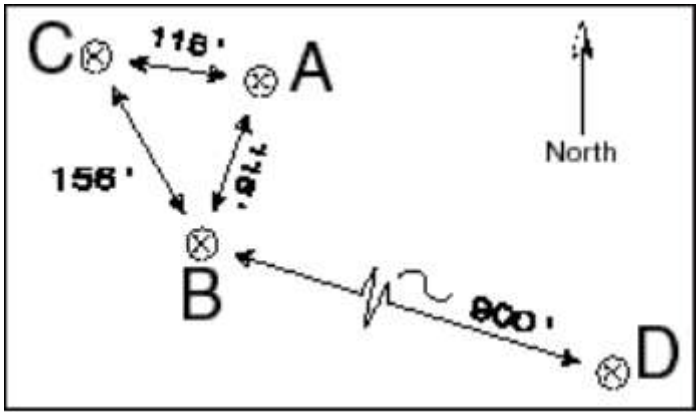

Figure 3 Geometrical site map (D-space) for intention-transmission experiments. Site A is the transmitting site (with IIED) while sites B, C, and D are receiving sites (no IIED), all located in different buildings.

oscillations appeared at site B that were highly correlated with A, but none were observed at site C or D[6]. Subsequent experiments of this type demonstrated that, as sites C and D became more conditioned, oscillation correlations appeared there as well. Further, the oscillation amplitude at site B (the receiver) was often larger than that at site A (the transmitter). However, in this latter case, only the vessel at site A was placed in a Faraday cage.

In this section, one needs to be very clear that R-space entanglement is very different than quantum entanglement. In quantum information science, groups of two or more quantum objects can have states that are entangled and these states can have properties unlike anything in classical physics. In classical information science, a familiar example is a string of bits, encoded via real physical objects like the spin of an atomic nucleus or the polarization of a photon of light but abstractly represented by 0's (down state) and 1's (up state). A qubit, the quantum version of a bit, has many more possible states called superposition states which entail both of these primary states but to varying degrees[14]. Since present-day quantum mechanics confines its formalism to a single four-space (distance-time) reference frame, quantum entanglement arises because the quantum "system" involves all these qubit states. In the present work, quantum considerations have not yet been built into the present formalism <u>which is a purely classical one</u> but, here, the

reference frame for viewing nature is now a biconformal base-space consisting of two, reciprocal four-dimensional sub-spaces where one of these subspaces is distance-time (D-space). Since the reciprocal subspace (R-space) is a wave space, the information wave space for D-space objects, our entanglement is due to the R-space superposition of this aspect of the defined "system". Thus, quantum entanglement and R-space entanglement have things in common, such as being connected with one another no matter how far apart the individual objects of the "system" are spaced, but they are fundamentally quite different.

(b) The Entangled System Perspective within a "Conditioned" Laboratory

If the laboratory has several different measurement stations but is only negligibly conditioned (the deltron-empowerment is negligible), then $Q_R << Q_D$ in Equation 2a and can be neglected in Q_M. Thus, the laboratory space is mostly uncoupled to the various measurement instruments located therein that are, in turn, uncoupled to each other. However, in a "conditioned" space, C_δ in Equation I-2a may be presumed to be large so that the different instrument measuring stations are coupled to each other and to the laboratory itself, considered as a general environment. Each of these D-space components has its own R-space part so one can no longer use Equation I-4 for a total equilibrium state answer. One must now take R-space superposition into account to find the system $\hat{FT}$; i.e.,

$$\hat{FT}_S = \hat{FT}_B + \sum_{j=1}^{n} \hat{FT}_j \qquad (4)$$

where the subscripts S, B and j refer to the total system, lab background and instrument measuring stations, respectively.

In Appendix III, the formal mathematical requirements of the "system of remote sites" logic is pursued. Here we will attempt a communication of the formal results with a minimum of mathematics.

When one evaluates the mathematical modulus for the entire system, $\hat{I}_{R_S}$, via the rule given by Equation I-3c which involves multiplying Equation 3 above by its complex conjugate, $\hat{FT}_S^*$, one obtains three terms in $\hat{I}^2_{R_S}$. The first is just the sum of the uncoupled $\hat{I}^2_{R_j}$. The second is an entanglement term between the lab background and the sum of all the j measuring stations while the third is just the sum of each measuring station with all the others. These entanglement products involve terms like $\hat{FT}_j \hat{FT}_k^*$ for two stations j and k. As a final step, one must integrate $\hat{I}^2_{R_S}$ over all of R-space to obtain the experimentally measured system result, Q_{R_S}, which is given by

$$Q_{R_S} = \int_{R-space} \hat{I}^2_{R_S}\, dk. \qquad (5a)$$

Using standard polar coordinate notation, $\hat{FT}_j = \hat{R}_j \exp(-i\hat{\theta}_j)$, as in Appendix III, $\hat{I}^2_{R_S}$ is given by

$$\hat{I}^2_{R_S} = \left[\hat{I}^2_B + \sum_{j=1}^{n} \hat{I}^2_j\right] + 2\hat{R}_B \sum_{j=1}^{n} \hat{R}_j \cos\left(\hat{\theta}_B - \hat{\theta}_j\right) + 2\sum_{j=1}^{n} \hat{R}_j \sum_{k\neq j}^{n} \hat{R}_k \cos\left(\hat{\theta}_j - \hat{\theta}_k\right) \qquad (5b)$$

The second and third terms on the right side of Equation 5b are the R-space entanglement contributions, discussed above, in terms of amplitudes, $\hat{R}_j$, and phase angles, $\hat{\theta}_j$.

Equation 5b above applies only if (a) all parts of the system are at the same physical location, (b) all parts are at the same EM gauge symmetry state and (c) all parts are of negligible size. How one removes each of these limitations is demonstrated in Appendix III. To illustrate these results, we consider the remote site experiment with n+1 sites and allow B to be replaced by C, the site to be treated as the origin of the system. Then we are looking at $\left(\hat{I}^C_{R_S}\right)^2$ from the perspective of location C so $\left(\hat{I}^C_{R_S}\right)^2$ replaces $\hat{I}^2_{R_S}$ in Equation 5b. Defining $\Delta\bar{r}_{jC}$ as the vector distance from the centroid of site j to the centroid of site C, Equation 5b retains the same form but the phase angle differences now become $[(\hat{\theta}_j - \hat{\theta}_C) + \Delta\bar{r}_{jC} \bullet \bar{k}_3]$ and $[(\hat{\theta}_j - \hat{\theta}_k) + (\Delta\bar{r}_{jC} - \Delta\bar{r}_{kC}) \bullet \bar{k}_3]$ where only the three spatial frequencies (k_x, k_y, k_z) are considered here. We will consider temporal frequencies, $\bar{k}_t$, below. When the C and j-spaces do not have the same EM gauge symmetry state, we invent gauge coupling parameters, α_{Cj}, between the C and j sites and, α_{jk}, between the j and k sites so Equation 5b, above, is altered by replacing $\hat{R}_j$ with $\alpha_{Cj}\hat{R}_j$ in the middle term and $\hat{R}_j$ with $\alpha_{jk}\hat{R}_j$ in the right hand term. We expect these α-values to be less than or equal to unity but always slightly greater than zero. For the moment these coupling coefficients must be determined by experiment. In Appendix III, Equation III-3b shows how to take account of non-negligible sizes for the various sites.

A much more interesting variation is the incorporation of time into the calculations. In this case, time must be included in the form of a fourth spatial coordinate, $x_4 = iv*t$, as utilized to prepare Figure 1. In general, there are two main

factors to be accounted for, (1) the R-space interference pattern due to multiple events (acting like objects) spaced along the x_4–coordinate and (2) the magnitude of the R-space "phantom" (reference 6, see Chapter 6, Figures 6.22-6.27) that may grow or decay with time in some manner. An illustration of these two factors can be seen by considering the repetitive 1-2 week cycles of (a) fresh water in the pH-measurement vessel at the beginning of the cycle (t=0), (b) continuous electronic pH-measurement for two-weeks and (c) replacement of this measured water plus electrode recalibration at the end of one or two weeks (t=τ). With the removal of this water, a "phantom" R-space profile is left in the vacuum at that particular x_4-coordinate and it decays (diffuses) at some unique rate depending upon the materials within the local environment. In fact, for an exact picture, we must include during this 0<t<τ period both a deltron incorporation reaction into the water from the environment, which increases its

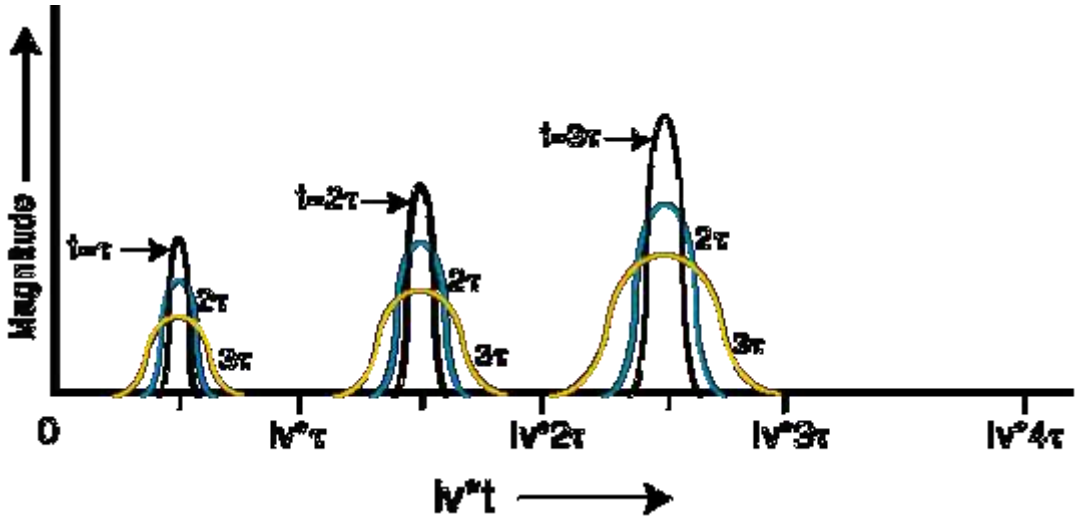

Figure 4. Gaussian-shaped phantoms generated during each pH measurement cycle.

pH, and a "phantom" decay reaction into the environment. However, for this paper, let us neglect this 0<t<τ dynamic and, for pedagogical purposes, presume that some Gaussian-shaped phantom generated during each cycle is placed at $x_4' = iv*\tau/2$, $x_4'' = iv*3\tau/2$, etc., and only begins to decay (broaden) after it has been initially generated. Thus, at some later point in time, a series of decaying Gaussian phantoms are centered in D-space and regularly spaced along the x_4-coordinate as illustrated in Figure 4.

All of these "phantoms" produce R-space interference with each other so that the system Fourier transform, $\hat{FT}_S$, is given by

$$\hat{FT}_S(t) = g_1(t - \tau/2)e^{ik'_t\bullet(t-\tau)} + g_2(t - 3\tau/2)e^{-ik'_t\bullet(t-2\tau)} + \cdots \qquad (6)$$

where g_n is the Gaussian for the nth cycle centered at $x_{4n} = iv^*\left[\tau/2 + (n-1)\tau\right]$ and $k_t' = 2\pi/t$ as noted earlier. The value of Q_R that comes from summing all these decaying Gaussians is what one expects to measure experimentally at any point in time. We also need to note that each Gaussian broadens into all four of the coordinate directions. Of course, to exactly match the multi-cycle data of Part I[12], it is necessary to go beyond this simple pedagogical example to a much more complex mathematical profile and that is beyond the scope of this paper.

Discussion

Equations 1a and 1b are quite similar at small times, $t \leq 0.3/\beta$ or $\sim 10^2 - 10^3$ seconds, where $\gamma \sim \beta\Delta$pH. One can show that ϕ varies approximately as $(k_t')^{-2}$ for constant n so it is low frequency values that are important here. Discontinuous jumps from n_i to n_j seem to be allowed but why the system might do so is not yet clear. Likewise, the proper choice for the magnitude of v* is not yet clear. One only knows that transformation from k_t' to k_t, an imaginary inverse spatial coordinate, is needed in order to obtain allowed mathematical solutions to the Equations delineated in Appendices I and II.

Figure 2 illustrates the importance of graininess in materials, how to define a system of many identical parts and how to go about calculating the FT for the entire system in terms of the FT for one of the parts. In the example discussed, a uniform disk-shaped type of granularity with infinitesimal thickness was utilized. In actuality, the triangle of material could be of monolayer thickness with identical atoms replacing the uniform disks. In a real material, structural and chemical defects will also be present (and must ultimately be accounted for since they are also part of the system which is the monolayer triangle). The procedure utilized here picked the centroid of the triangle as the origin for our reference frame. This is the type of approximation used in developing all the subsequent equations on R-space entanglement.

Although it is beyond the scope of the present paper, it is worth noting here that the centroid of the triangle is on the surface of the earth so it is rotating with respect to a reference frame (RF) tied to the center of the earth. This new RF is rotating with respect to a RF tied to the center of the sun that is, in turn, rotating and translating relative to a RF in the Milky Way. Further, if indeed the "stuff" of R-space is at the vacuum level of substance[12] then, the Michalson-Moreley experiment not withstanding, some relative change may also occur between the R-space RF and this D-space RF and that it must be accounted for in an exact solution.

In analogy to Figure 3, the total "remote site" experiment encompasses at least the seven sites illustrated in Figure 5. The P, K and M sites also have satellite "control" sites associated with them while the S-site only functioned from January 1, 1997 to September 1 1997 and the M^*_{I1}-site only functioned from September 1, 1997 to March, 2000. Thus, if Equation III-3b is used to represent this remote site experimental system

Figure 5. Geographical location of the various experimental sites involved in the IIED experiments:

1. P = Payson master site (06/00-present)
2. S = Stanford site (01/97-09/97)
3. M* = Minnesota site (09/97-03/00)
4. K = Kansas site (12/01-present)
5. M = Missouri site (12/01-present)
6. B_1 = Bethesda site (4/02-present)
7. B_2 = Baltimore site (4/02-present)

and, if we can approximate $\hat{FT}_j$ by the product of a spatial related part and a temporal related part (when the separation of variables procedure holds), something like Equation 5 must be a part of $\hat{FT}_j$ in Equation III-3b ($\hat{FT}_j \approx \hat{FT}_j(\bar{k}_3)\hat{FT}_j(k_t)$). This means that past temporal events at one site of the system can produce an "entangled" contribution at another site of the system in present time. Of course, $\hat{FT}_S{}^C$ must then be converted to $\hat{I}_{RS}{}^C(k_4)$ and then $(\hat{I}_{RS}{}^C)^2$ integrated over the four R-space coordinate directions to obtain the total R-space measurement contribution at C, Q_R^C.

The concept of R-space entanglement can be most readily appreciated by considering a system of only two parts, A and B, where $\hat{FT}_S = \hat{FT}_A + \hat{FT}_B$ and $\hat{I}_{RS}{}^2 = (\hat{FT}_A + \hat{FT}_B)(\hat{FT}_A{}^* + \hat{FT}_B{}^*) = \hat{I}_A{}^2 + \hat{I}_B{}^2 + \varepsilon_{AB}$ where ε_{AB} is the entanglement

given by $\varepsilon_{AB} = \hat{FT}_A \hat{FT}_B^* + \hat{FT}_A^* \hat{FT}_B$, a type of cross-product between A and B. If one is conducting a double blind medical study and, to first order, can neglect the human practitioner effect, then the system devolves to a treatment contribution (A) and a placebo contribution (B). In this case, one sees that ε_{AB} involves both contributions and, approximately, the magnitude of the placebo effect is linearly related to the magnitude of the treatment effect.

Our perspective on "the system" is broadened when we consider the famous double slit experiment for electrons. It is well known that, in the classical experiment when one has no knowledge of which slit any single electron will go through, a well-defined diffraction pattern exists on the screen behind the slits. This is to be expected because the "system" is two slits with electrons so they interfere with each other via an ε_{AB}-type of entanglement. However, when photons illuminate the electrons so that one has information regarding which slit a particular electron will go through then, for such electrons, the "system" is only a single slit and one observes a strong intensity contribution on the screen only directly behind the two slits. We thus see how careful one must be here in <u>defining what constitutes the system</u>.

This perspective is somewhat further broadened when we consider the two human EEG experiments of reference 15. Here, two humans (A and B) are wired up for EEG monitoring and placed in rooms some distance apart. Light stimulation on the closed eyelids of one subject, A, produces a readily distinguishable signature in A's brain waves. Such a signature was also looked for in the brainwaves of B. It was not found! However, when subjects A & B were first allowed to meditate together (side by side) for ~ 10 minutes before the EEG experiment was repeated, then the EEG signature was found in B's brain waves when A's eyelids were light-stimulated. Thus, one sees that a special kind of linkage procedure was needed for A and B to become R-space entangled.

For our final example, here, let us pick a remote object at some coordinate location (x_1, x_2, x_3, x_4) and an observer (participant) who seeks to describe the object in some detail located at coordinates (x_1', x_2', x_3', x_4'). If the observer's intent is sufficient, then the object and the observer form a system A + B and $\hat{FT}_S = \hat{FT}_A + \hat{FT}_B$ so that $\hat{I}_{RS}^{\,2}$ contains an entanglement contribution for the object, $\hat{FT}_A$, in the observer's R-space information gathering system. The translation operator needed to transfer $\hat{FT}_A$ to the observer's coordinate position, $\exp[i(k_x\Delta x_1 + k_y\Delta x_2 + k_z\Delta x_3 + k_t'\Delta x_4)]$ is readily calculable and thus presumably also calculable by the unconscious mind of the observer. Thus, $\hat{FT}_A$ appears to be accessible to the brain of the observer where an inverse FT-operation yields the pattern and dimensions of the remote object.

The last point to be reemphasized is that this information entanglement process is a purely classical process wherein one changes reference frames from our

single distance-time RF to the particular biconformal base-space RF used here. No quantization of any sort has yet been included in this model.

Acknowledgements

We wish to thank Ditron, LLC and the Samueli Institute for partial support of this work.

References

1. Tiller, W.A., Science and Human Transformation: Subtle Energies, Intentionality and Consciousness (Pavior Publishing, Walnut Creek, 1997) pp. 264 – 273.

2. Tiller, W.A. (1993). What are Subtle Energies? *Journal of Scientific Exploration,* 7, 293.

3. Tiller, W.A. (1999) "Subtle Energies" Science and Medicine 1:28

4. Tiller, W.A. and Dibble, W.E., Jr. (2001) "New experimental Evidence Revealing an Unexpected Dimension to Materials Science and Engineering" Materials Research Innovation, 5, 21-34.

5. Kohane M.J. and Tiller W.A. (2001) "Quantum Mechanics and Electromagnetic Fields: The Possibility of Device-encapsulated Human Intention in Medical Therapies", Medical Hypotheses 56 (6) 598-607.

6. Tiller, W.A., Dibble, W.E., Jr. and Kohane M.J. (2001), Conscious Acts of Creation: The Emergence of a New Physics (Pavior Publishing, Walnut Creek, CA).

7. Tiller, W.A. (2002) "The Real World of Modern Science, Medicine and Qigong", Bulletin of Science, Technology and Society, 22 (5), 352.

8. Tiller, W.A. (2003) "A Personal Perspective on Energy Medicine and Whole Person Healing" J. Alternative and Complementary Medicine, Special Energy Issue.

9. Tiller, W.A. (2003) "A Multidimensional Model Capable of Accommodating the New Data", Proceedings of the First International Conference on Whole Person Healing, Bethesda, MD, March 2003.

10. Gerber, R. (1988) Vibrational Medicine (Bear and Company, Santa Fe, NM).

11. Oschman, J.L. (2000) Energy Medicine: The Scientific Basis (Churchill Livingstone, Edinburgh, U.K.).

12. Tiller, W.A., Dibble, W.E., Jr., Nunley, R.E. and Shealy, C.N. (2003), "Towards General Experimentation and Discovery in 'Conditioned' Laboratory Spaces, Part I: Experimental pH-Change Findings at Some Remote Sites", Submitted to J. Alternative and Complementary Medicine, Special Energy Issue.

13. Tiller, W.A., Dibble, W.E., Jr., Rollwagen, F., Cheng, H., Ives, J., Jonas, W., Shealy, C.N. and Nunley, R. (2003) "Towards General Experimentation and Discovery in 'Conditioned' Laboratory Spaces, Part II: pH-change Experience at Four Remote Sites, One-year Later", Submitted to J. Alternative and Complementary Medicine, Special Energy Issue.

14. Nielsen, M.A. (2002) "Rules for a Complex Quantum World", Scientific American, 287 (5), 67.

15. Grindberg-Zylberbaum, J., Delaflor, M., Attie, L., and Goswami, A. (1994) Physics Essays, 7, 422.

Appendix I: Solving for the Allowed R-space Solutions to Equation 2c of the Main Text

From the main text, we have

$$Q_{M_{pH}} = Q_{D_{pH}} + Q_{R_{pH}}\,, \tag{I-1a}$$

where

$$Q_{D_{pH}} \approx pH_0 \text{ and } Q_{R_{pH}} \approx \Delta pH(1-e^{-\beta t}) \tag{I-1b}$$

The Fourier-pair relationships, in one dimension, for our type of biconformal base-space are, assuming equilibrium holds between the reciprocal spaces,

$$\hat{FT}(k_t) = \frac{1}{(2\pi)^{1/2}} \int_{D-space} Q_D(t)\, C_\delta(t,k_t\cdots) e^{it\bullet k_t} dt \tag{I-2a}$$

and

$$Q_D(t)C_\delta(t,k_t\cdots)=\frac{1}{(2\pi)^{1/2}}\int_{R-space}\hat{FT}(k_t)e^{-it\bullet k_t}dk_t. \qquad \text{(I-2a)}$$

Here, C_δ is the unknown deltron activation function which leads to the empowered Fourier transform, $\hat{FT}$ (the ^ over FT designates this empowerment factor). In general, $\hat{FT}(k_t)$ is a vector given by

$$\hat{FT}(k_t)=\hat{R}(k_t)e^{i\hat{\theta}(k_t)} \qquad \text{(I-3a)}$$

where $\hat{R}$ is the vector amplitude as a function of the R-space coordinate, k_t, and $\hat{\theta}$ is the vector phase angle relative to the abscissa in a plot of $\hat{FT}$ vs. k_t. The complex conjugate of $\hat{FT}(k_t)$, denoted $\hat{FT}^*(k_t)$ is just the mirror reflection of $\hat{FT}(k_t)$ in the abscissa so that

$$\hat{FT}^*(k_t)=\hat{R}(k_t)e^{-i\hat{\theta}(k_t)}. \qquad \text{(I-3b)}$$

The empowered mathematical modulus, or amplitude, $\hat{I}_R$ is just given by

$$\hat{I}_R(k_t)=[\hat{FT}\hat{FT}^*]^{1/2}=\hat{R}(k_t), \qquad \text{(I-3c)}$$

and the experimentally measured contribution is given by

$$Q_R=\int_{R-space}\hat{I}_R^2(k_t)dk_t=\Delta pH(1-e^{-\beta t}) \qquad \text{(I-4)}$$

Thus, the mathematical task is to work with Equation I-4, extract $\hat{I}_{R_{pH}}^2$ and then plot this (amplitude)^2 profile. To do this, just as in relativity theory, one must first convert the D-space time-coordinate to the imaginary spatial form, iv*t, where v* is a spatial velocity. We use v* instead of c, the velocity of light as used in relativity theory, because v* is the velocity of our reference frame (the moving earth) relative to the cosmos. More generally, we can simply allow v* to be an undetermined parameter of our problem and $k_t'=2\pi/t$ is replaced by $k_t=-2\pi/v^*t$. Thus, dividing Equation I-4 by $(2\pi)^{1/2}$ and k_t to k_t', we obtain

$$\frac{\Delta pH(1-e^{-\beta t})}{(2\pi)^{1/2}} = \frac{1}{(2\pi)^{1/2}} \int_{R-space} \left[\hat{I}^{2}_{R_{pH}} e^{it\bullet k'_t} \right] e^{-it\bullet k'_t} d\left(\frac{-i}{v^*} k'_t \right) \qquad \text{(I-5)}$$

So, via Equation I-2b, $[\Delta pH/(2\pi)^{1/2}][1-e^{-\beta t}]$ is the inverse Fourier transform of $[\hat{I}^{2}_{R} e^{it\bullet k'_t}]$ so the latter is the Fourier transform of the former; i.e.,

$$-\left(\frac{i}{v^*}\right)\hat{I}^{2}_{R} e^{it\bullet k'_t} = \frac{1}{(2\pi)^{1/2}} \int_{D-space} \frac{\Delta pH(1-e^{-\beta t})}{(2\pi)^{1/2}} e^{it\bullet k'_t} dt \qquad \text{(I-6a)}$$

$$= \frac{\Delta pH}{2\pi} \left\{ \frac{e^{it\bullet k'_t}}{ik'_t}\Big|_0^t - \frac{e^{t(ik'_t-\beta)}}{(ik'_t-\beta)}\Big|_0^t \right\} \qquad \text{(I-6b)}$$

Using the definitions, $x = tk'_t$ and $y = k'_t/\beta$, Equation I-6b becomes

$$\left(\frac{-i}{v^*}\right)\hat{I}^{2}_{R_{pH}} e^{ix} = \frac{\Delta pH}{2\pi\beta} \left\{ \frac{1-e^{\left(ix-\frac{x}{y}\right)}}{(iy-1)} - \frac{\left(1-e^{ix}\right)}{iy} \right\} \qquad \text{(I-7a)}$$

$$= \frac{\Delta pH}{2\pi\beta} \left\{ \frac{(-iy-1)\left(1-e^{\left(ix-\frac{x}{y}\right)}\right)}{\left(y^2+1\right)} + \frac{iy}{y^2}\left(1-e^{ix}\right) \right\} \qquad \text{(I-7b)}$$

$$= \frac{\Delta pH}{2\pi\beta} \left\{ \frac{(i-y)+\left[y(1+iy)e^{\left(-\frac{x}{y}\right)} - i\left(1+y^2\right)\right]e^{ix}}{y\left(1+y^2\right)} \right\}. \qquad \text{(I-7c)}$$

Equating real parts from both sides and imaginary parts from both sides yields the two equations

$$\hat{I}_{R_{pH}}^{2}\,\frac{\sin x}{v^{*}}=\frac{\Delta pH}{2\pi\beta}\left\{\frac{-y+ye^{\left(-\frac{x}{y}\right)}\cos x-y^{2}e^{\left(-\frac{x}{y}\right)}\sin x+\left(1+y^{2}\right)\sin x}{y\left(1+y^{2}\right)}\right\} \qquad \text{(I-8a)}$$

and

$$-\hat{I}_{R_{pH}}^{2}\,\frac{\cos x}{v^{*}}=\frac{\Delta pH}{2\pi\beta}\left\{\frac{1+y^{2}e^{\left(-\frac{x}{y}\right)}\cos x+ye^{\left(-\frac{x}{y}\right)}\sin x-\left(1+y^{2}\right)\cos x}{y\left(1+y^{2}\right)}\right\}. \qquad \text{(I-8b)}$$

Dividing Equation I-8a by I-8b yields

$$-\tan x=\left\{\frac{-y+[y\cos x-y^{2}\sin x]e^{-\frac{x}{y}}+\left(1+y^{2}\right)\sin x}{1+\left(y^{2}\cos x+y\sin x\right)e^{-\frac{x}{y}}-\left(1+y^{2}\right)\cos x}\right\}. \qquad \text{(I-9)}$$

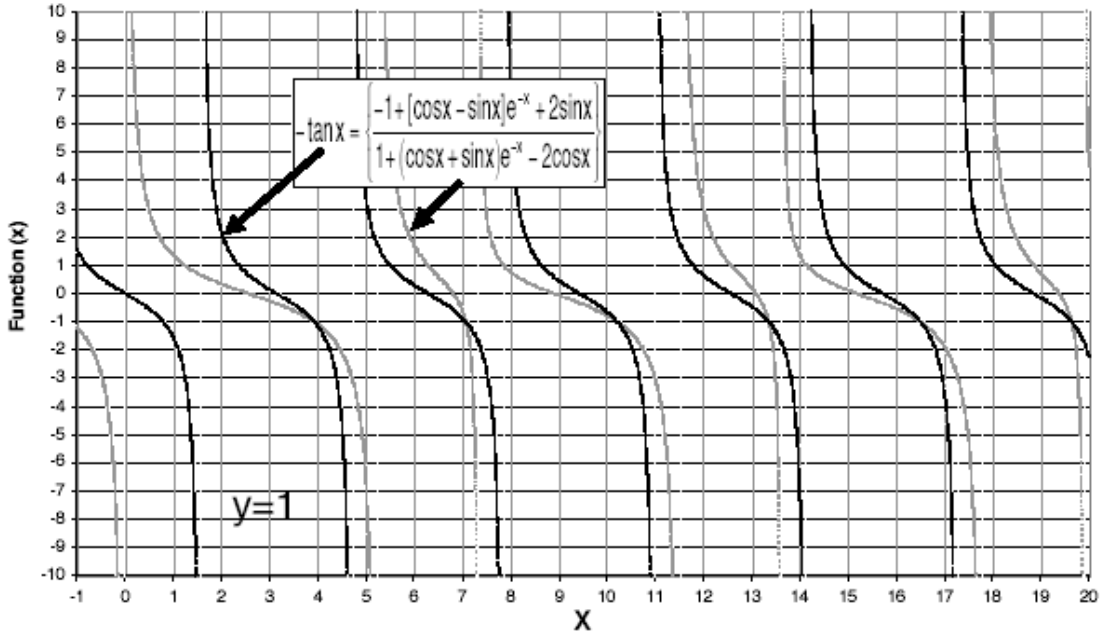

Figure Ia. Multiple y=1 solutions for tan(x) from Equation I-9. The RHS of Equation I-9 is depicted by gray curves. There are no negative x solutions.

Thus, for every value of y on the right, Equation I-9 yields a value for x. As can be seen from choosing y=1, Equation I-9 yields multiple solutions for -tan x illustrated by the intersection points in Figure Ia. Here -tan x is given by the bold curves while the RHS of Equation I-9 is given by the gray curves. Figure Ib provides plots of the first five allowed x-values, with the first solution giving x=4 at y=1, for a range of y. From Equation I-8a, $\phi = \hat{I}^2_{R_{pH}} \beta/v^*\Delta pH$ can now be readily calculated as a function of $y = k'_t/\beta$ for the multiple x-solutions (n=1, 2,…). These plots for n from 1 to 5 are given in Figure 1 of the main text.

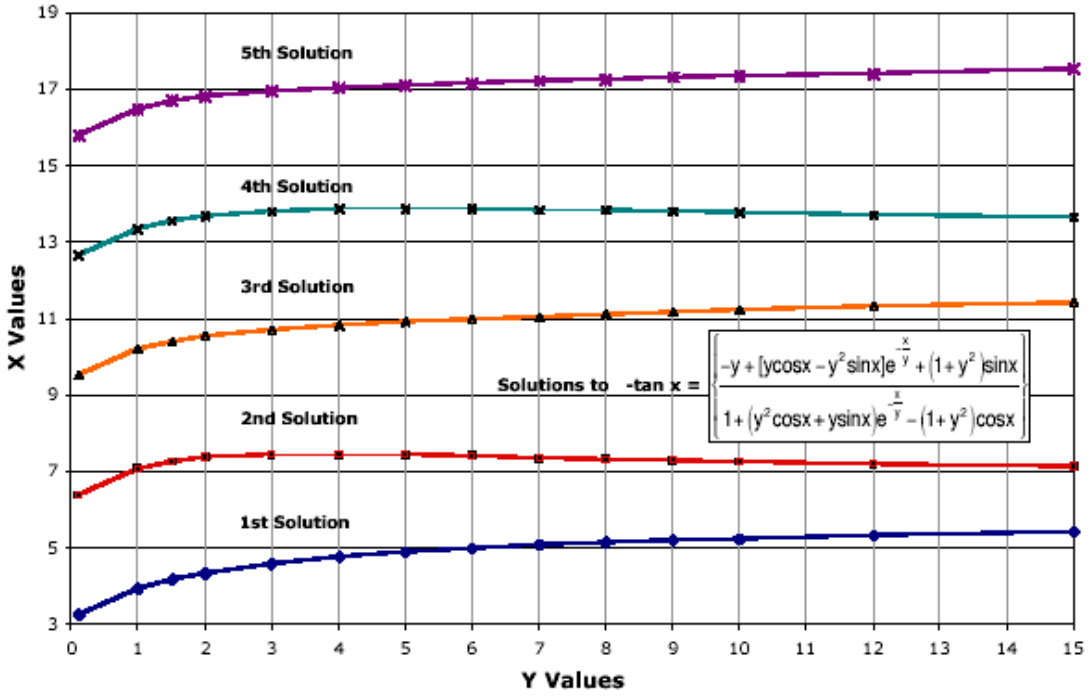

Figure Ib. Multiple solutions for x as a function of y from Equation I-8a.

Since we now know $\hat{I}_{R_{pH}} = [\phi\, v^{*}\Delta pH\, /\beta]^{1/2}$, we have $\hat{R}_{pH}(k'_t)$ but do not know $\hat{\theta}(k'_t)$ in Equation I-3a; thus, we are unable to obtain $C_\delta(t, k'_t, \cdots)$ from Equation I-2b without such phase angle information; i.e., here , we find that

$$C_\delta(t,k'_t\cdots) = \frac{[\phi v * \Delta pH/\beta]^{1/2}}{(2\pi)^{1/2} pH_0} \int_{R-space} e^{i\hat{\theta}(k'_t)} e^{-it\bullet k_t} dk_t \qquad \text{(I-10)}$$

Appendix II: From Equation 2d to $\hat{I}^2_{R_{pH}}(k'_t)$

Beginning with Equation 2d of the main text, this requires that

$$\left(\frac{-i}{v^*}\right)\hat{I}^2_{R_{pH}} e^{itk'_t} = \frac{1}{(2\pi)^{1/2}}\int_D \frac{\gamma t}{(2\pi)^{1/2}} e^{itk'_t} dt, 0 \le t \le t_1 \qquad \text{(II-1a)}$$

$$= \frac{\gamma}{2\pi}\left\{\frac{e^{itk'_t}}{k'^2_t}(1 - itk'_t) - \frac{1}{k'^2_t}\right\}. \qquad \text{(II-1b)}$$

Defining $x = k'_t t$, Equation II-1b yields, when expanded into real and imaginary parts,

$$\hat{I}^2_{R_{pH}} \frac{\sin x}{v^*} = \frac{\gamma t^2}{2\pi}\left\{\frac{\cos x - 1 + x\sin x}{x^2}\right\} \qquad \text{(II-2a)}$$

and

$$-\hat{I}^2_{R_{pH}} \frac{\cos x}{v^*} = \frac{\gamma t^2}{2\pi}\left\{\frac{\sin x - x\cos x}{x^2}\right\}. \qquad \text{(II-2b)}$$

Dividing Equation II-2a by Equation II-2b gives

$$-\tan x = \left\{\frac{\cos x + x\sin x - 1}{\sin x - x\cos x}\right\} \qquad \text{(II-3)}$$

which has the simple solution

$$\cos x = 1. \qquad \text{(II-4)}$$

Equation II-4 is satisfied only for $x = 2n\pi$ ($n = 0, \pm 1, \pm 2, \ldots$) so Equation II-2b yields

$$\hat{I}^2_{R_{pH}} \approx \frac{v^* \gamma t^2}{2\pi(n+1)} \quad \text{for } n = 0, \pm 1, \pm 2, \ldots) \text{ and } 0 \le t \le \tau. \qquad \text{(II-5)}$$

The RHS of Equation II-5 has units of pH-cm.

Appendix III: R-space Entanglement between Remote Sites

Biconformal base-space theory shows that there are two contributions, Q_D and Q_R, to any physical measurement, Q_M, i.e.,

$$Q_M = Q_D + Q_R = Q_D + \int_R \hat{FT}_S \hat{FT}_S^* dk \qquad \text{(III-1a)}$$

where $\hat{FT}_S$ is the equilibrium deltron-empowered Fourier transform for the D-space "system" of parts while $\hat{FT}_S^*$ is its complex conjugate. Thus, for a system of N meaningfully interacting R-space parts, superposition of the isolated $\hat{FT}$ s gives

$$\hat{FT}_S = \sum_{j=1}^{N} \hat{FT}_j = \sum_{j=1}^{N} \hat{R}_j e^{i\hat{\theta}_j} \qquad \text{(III-1b)}$$

where, in the right hand polar coordinate expression, R_j is the amplitude and θ_j is the phase angle for the vector, j. Thus, we have

$$\hat{FT}_S \hat{FT}_S^* = \sum_{j=1}^{N} \hat{R}_j e^{i\hat{\theta}_j} \sum_{j=1}^{N} \hat{R}_j e^{-i\hat{\theta}_j} = \sum_{j=1}^{N} \hat{R}_j^2 + 2\sum_{j=1}^{N} \sum_{l\neq j=1}^{N} \hat{R}_j \hat{R}_l \cos\left(\hat{\theta}_j - \hat{\theta}_l\right), \qquad \text{(III-1c)}$$

and this cross-product term on the far right is the R-space entanglement contribution of one part of the system with another. As it stands, Equation III-1c only applies if (1) all parts of the system are at the same physical location, (2) are in the same EM gauge symmetry state and (3) are of negligible spatial extent. Let us now remove these limitations one by one.

(1) Location Differences Relaxed: Let us consider site j=C as our measurement site for consideration and we want to know the effect of the rest of the system (j≠C) at site C. Thus, in our $\hat{FT}_S$ from the perspective of Site C, designated $\hat{FT}_S{}^C$, we must perform a simple linear transformation of each j≠C site to the actual position of site C via Equation 8 of the main text to position j. Defining $\Delta\bar{r}_{jc}$ as the vector distance from the centroid of site j to the centroid of site C, Equation III-1b becomes

$$\hat{FT}_S{}^C = \hat{FT}_C + \sum_{j\neq C}^{N-1} \hat{FT}_j e^{i\Delta\bar{r}_{jc}\bullet\bar{k}} \qquad \text{(III-2a)}$$

$$= \hat{FT}_C + \sum_{j\neq C}^{N-1} \hat{R}_j e^{i\left[\hat{\theta}_j + \Delta\bar{r}_{jc}\bullet\bar{k}\right]} \qquad \text{(III-2b)}$$

and

$$\hat{FT}_S{}^C \hat{FT}_S{}^{C*} = \hat{R}_C^2 + \sum_{j\neq C}^{N-1} \hat{R}_j^2 + 2\hat{R}_C \sum_{j\neq C}^{N-1} \hat{R}_j \cos\left[\left(\hat{\theta}_j - \hat{\theta}_C\right) + \Delta\bar{r}_{jC} \bullet \bar{k}\right]$$

$$+ 2 \sum_{j\neq C}^{N-1} \sum_{l\neq j\neq C}^{N-2} \hat{R}_j \hat{R}_l \cos\left[\left(\hat{\theta}_j - \hat{\theta}_l\right) + \left(\Delta\bar{r}_{jC} - \Delta\bar{r}_{lC}\right) \bullet \bar{k}\right] \qquad \text{(III-2c)}$$

(2) Negligible Size Relaxed: Equations III-2 hold for all points in site j relative to the centroid of site C so we need to perform an integration over the volume of site j. We will assume, for simplicity, that the three dimensional space is of rectangular parallelepiped shape with dimensions [$2L_{xj}$ x $2L_{yj}$ x $2L_{zj} = V_j$ = volume of j]. For this case, we must have

$$\hat{FT}_S{}^C = \hat{FT}_C$$

$$+ \sum_{j\neq C}^{N-1} \left\{ e^{i\Delta\bar{r}_{jC} \bullet \bar{k}} \int_{-L_{Sj}}^{L_{Sj}} e^{i\left(x'k_x + y k_y + z' k_z\right)} \hat{FT}_j \left(x_{0j} + x'_j ; y_{0j} + y'_j ; z_{0j} + z'_j\right) dx'_j \, dy'_j \, dz'_j \right\} \quad \text{(III-3a)}$$

where S_j = x'_j, y'_j, z'_j and x_{0j}, y_{0j}, z_{0j} are the coordinates for the centroid of j. If we assume that the $\hat{FT}_j$ are spatially homogeneous rather than spatially heterogeneous, these integrals are easily solved to yield

$$\hat{FT}_S{}^C = \hat{FT}_C + \sum_{j\neq C}^{N-1} V_j \left\{ e^{i\Delta\bar{r}_{jC} \bullet \bar{k}_3} \left(\frac{\sin k_x L_{xj}}{k_x L_{xj}} \right) \left(\frac{\sin k_y L_{yj}}{k_y L_{yj}} \right) \left(\frac{\sin k_z L_{zj}}{k_z L_{zj}} \right) \right\} \hat{FT}_j. \quad \text{(III-3b)}$$

(3) Same EM Gauge Symmetry Relaxed: When the C- and j-spaces do not have the same EM gauge symmetry state, as a zeroth order approximation, we can incorporate a parametric coupling coefficient $0 \leq \alpha_{Cj} \leq 1$ multiplying $\hat{FT}_j$ to give α_{Cj} $\hat{FT}_j$ instead of just $\hat{FT}_j$ in Equation III-3b. Thus, the R-space contribution to any physical measurement at C is given by

$$Q_R{}^C = \int_R \hat{F}T_S{}^C \hat{F}T_S{}^{C*} d\bar{k}_3 \qquad \text{(III-4)}$$

The parameter α_{Cj} is the one we know least about but we can expect it to be very nonlinear, going from ~0 when site C is in the U(1) EM gauge state while site j is in the SU(2) EM gauge state and going to ~1 when both are in the SU(2) EM gauge state. However, it appears possible that the α_{Cj} may be determinable from experiment.